Acta Biochim Biophys Sin 2022, 54(1): 126–136
https://doi.org/10.3724/abbs.2021005
Advance Access Publication Date: 28 December 2021
Original Article

Original Article

miR-30a-5p promotes glomerular podocyte apoptosis via DNMT1-mediated hypermethylation under hyperhomocysteinemia

Ning Ding[1,2,3], Lin Xie[1,2,3], Fei Ma[1,2,3], Shengchao Ma[1,2,3], Jiantuan Xiong[1,2,3], Guanjun Lu[2,3,4], Huiping Zhang[2,3,5,*], and Yideng Jiang[1,2,3,*]

[1]School of Basic Medical Sciences, Ningxia Medical University, Yinchuan 750004, China, [2]NHC Key Laboratory of Metabolic Cardiovascular Diseases Research, Ningxia Medical University, Yinchuan 750004, China, [3]Ningxia Key Laboratory of Vascular Injury and Repair Research, Ningxia Medical University, Yinchuan 750004, China, [4]Department of Clinical Medicine, General Hospital of Ningxia Medical University, Yinchuan 750004, China, and [5]Prenatal Diagnosis Center, General Hospital of Ningxia Medical University, Yinchuan 750004, China
*Correspondence address. Tel: +86-951-6743137; E-mail: zhp19760820@163.com (H.Z.) / Tel: +86-951-6980007; E-mail: jydeng@nxmu.edu.cn (Y.J.)

Received 10 August 2021 Accepted 14 September 2021

Abstract

Abnormal elevation of homocysteine (Hcy) level is closely related to the development and progression of chronic kidney disease (CKD), with the molecular mech2anisms that are not fully elucidated. Given the demonstration that miR-30a-5p is specifically expressed in glomerular podocytes, in the present study we aimed to investigate the role and potential underlying mechanism of miR-30a-5p in glomerular podocyte apoptosis induced by Hcy. We found that elevated Hcy downregulates miR-30a-5p expression in the *Cbs*$^{+/-}$ mice and Hcy-treated podocytes, and miR-30a-5p directly targets the 3′-untranslated region (3′-UTR) of the forkhead box A1 (FOXA1) and overexpression of miR-30a-5p inhibits FOXA1 expression. By nMS-PCR and MassARRAY quantitative methylation analysis, we showed the increased DNA methylation level of miR-30a-5p promoter both *in vivo* and *in vitro*. Meanwhile, dual-luciferase reporter assay showed that the region between –1400 and –921 bp of miR-30a-5p promoter is a possible regulatory element for its transcription. Mechanistic studies indicated that DNA methyltransferase enzyme 1 (DNMT1) is the key regulator of miR-30a-5p, which in turn enhances miR-30a-5p promoter methylation level and thereby inhibits its expression. Taken together, our results revealed that epigenetic modification of miR-30a-5p is involved in glomerular podocyte injury induced by Hcy, providing a diagnostic marker candidate and novel therapeutic target in CKD induced by Hcy.

Key words miR-30a-5p, DNA methylation, podocyte apoptosis, FOXA1

Introduction

Chronic kidney disease (CKD) is a worldwide health issue which can progress to advanced renal failure, end-stage renal disease, and even death, while effective treatment of CKD is still lacking. Abnormal elevated plasma homocysteine (Hcy) concentrations (tHcy > 15 μM) are known as hyperhomocysteinemia (HHcy), which is considered as a risk or pathogenic factor in the progression of CKD as well as the cardiovascular complications [1,2]. Multiple reports have shown that HHcy accelerates the progression of CKD by regulating oxidative stress, endoplasmic reticulum stress and inflammation [3–5]. However, improved understanding of the role of HHcy in CKD is necessary for better treatment. Glomerular podocytes are a group of highly differentiated glomerular epithelial cells with poor proliferation capability, which play a critical role in the maintenance of the glomerular filtration barrier integrity [6]. Injury and loss of glomerular podocytes caused by various stresses and pathological stimuli are critical for the pathogenesis of proteinuria and CKD [7]. Therefore, CKD can benefit from protecting glomerular podocytes from injury and limiting their loss.

MicroRNAs (miRNAs) are endogenous, non-coding small RNAs with 21–24 nucleotides long. They play important roles in various biological processes through negative modulation of gene expression after post-transcription [8]. It has been demonstrated that abnormal expressions of miRNAs play a pivotal role in CKD. For instance, miR-193a, miR-34a, and miR-195 promote glomerular podocyte injury [9–11]. In contrary, miR-29a, miR-217 and miR-590 can protect podocytes from injury [12–14]. miR-30a-5p is a member of the miR-30 family which has five members of distinct pre-mature

miRNAs, showing diverse roles in the regulation of tumorigenesis, metastasis, chemo-resistance and clinical prognosis in several types of human cancers [15]. Accumulating studies have suggested that miR-30a-5p, which is specifically expressed in the cells of collecting duct and podocytes, is a biomarker in the urine of patients with focal segmental glomerular sclerosis [16,17]. Therefore, it would be interesting to know whether Hcy promotes glomerular podocyte injury through the regulation of miR-30a-5p as well.

DNA methylation is one of the major epigenetic modifications that can activate or repress gene expression. Numerous studies have demonstrated that DNA methylation plays a key role in the silencing of genes that are involved in cellular processes, such as cell cycle checkpoint, cell apoptosis, signal transduction, cell adhesion and angiogenesis [18,19]. Hcy is a sulfur-containing non-protein forming amino acid synthesized during methionine metabolism and it is a byproduct of cellular methylation reactions, which serves as a sensitive marker of one-carbon metabolism important for multiple physiological processes, including DNA methylation regulation [20]. Our previous studies showed that Hcy causes aberrant DNA methylation and impairs epigenetic control of gene expression, suggesting that epigenetic dysregulation of gene expression mediated by DNA methylation is a pathogenic consequence of HHcy in many human diseases [21]. DNA methylation of mi RNAs has been identified as an emerging mechanism of miRNA regulation. In particular, the hypermethylation of the miRNA promoter has been recognized as a mechanism leading to dysregulation of miRNA expression in cancers [22–24]. These studies implied that DNA methylation is an important cofactor for miRNA expression.

In the present study, we identified that miR-30-5p is associated with podocyte apoptosis during Hcy-induced glomerular injury. Mechanistic studies demonstrated that DNMT1 mediates miR-30-5p promoter hypermethylation to suppress its expression, thus regulates FOXA1 expression in glomerular podocyte injury induced by Hcy. Our work provides new insights into the molecular mechanisms of the development of HHcy-induced CKD, and a potential strategy for its diagnosis and treatment.

Materials and Methods

Ethical compliance

All animal experiments were performed according to guidelines approved by the Institutional Animal Care and Use Committee of the Ningxia Medical University, and the ethics approval number is 2018-089.

Experimental animals

Cystathionine beta-synthase (Cbs) heterozygous knockout ($Cbs^{+/-}$) mice (8–10 weeks old) were purchased from Jackson Laboratory (Bar Harbor, USA) and maintained in the Ningxia Medical University Laboratory Animal Center. Mice were housed in a controlled environment on the 12/12 h light/dark cycle. Mice genotypes were determined by a PCR of DNA from tail biopsies with a specific set of primers. $Cbs^{+/+}$ and $Cbs^{+/-}$ mice were used in the experiments since Cbs homozygote knockout ($Cbs^{-/-}$) mice have a short life span and die of liver failure before weaning, and all mice were fed with chow diet plus 2% methionine diet for 8 weeks to induce HHcy. For the overexpression assay, $Cbs^{+/-}$ mice were randomly assigned into the following 3 groups: PBS, AAV9-miR-neg, and AAV9-miR-30a-5p (GENE, Shanghai, China). PBS group mice were injected with 100 μL PBS into left renal, AAV9-miR-neg group mice were injected with 100 μL miRNA negative control (10 μL miR-neg + 90 μL PBS) into left renal, and AAV9-miR-30a-5p group mice were injected with miR-30a-5p adeno-associated virus (10 μL AAV9-miR-30a-5p + 90 μL PBS) into left renal.

Cell culture and transfection

Conditionally immortalized mouse podocytes (MPC-5) and human HEK293 cells (h243) were obtained from iCell Bioscience Inc. (Shanghai, China). Podocytes and HEK293 cells were grown in Dulbecco's modification of Eagle's medium (DMEM) (GIBCO, New York, USA) containing 10% fetal bovine serum (GIBCO), 1% penicillin-streptomycin, and incubated at 37°C with 5% CO_2. After cell cultures reached a confluence of 70%–80%, podocytes were treated with 80 μM Hcy (Sigma-Aldrich, Darmstadt, Germany) for 48 h. For transfection experiments, miR-30a-5p inhibitor, miR-30a-5p mimic, miRNA negative control (miR-neg), and small interfering RNAs (siRNAs) specifically targeting DNA methyltransferase enzyme 1 (si-DNMT1) were obtained from Gene Pharma (Shanghai, China). Recombinant adenoviruses expressing DNMT1 (Ad-DNMT1) were purchased from HANBIO (Shanghai, China). Then, the cells were seeded in 6-well plates and transfected according to the supplier's instructions. The siRNA sequences of DNMT1 are as follows: si-NC: 5′-UUCUCCGAACGUGUCACGUTT-3′; si-DNMT1-1: 5′-GCAAAGAG UAUGAGCCAAUTT-3′; si-DNMT1-2: 5′-GCUGGUCUAUCAGAUCU UUTT-3′, and si-DNMT1-3: 5′-CCGAGGCCUUUACUUUCAATT-3′.

Transmission electron microscopy (TEM)

Biopsy from kidney tissues were cut into pieces (1 mm × 1 mm × 5 mm), and fixed with glutaraldehyde at 4°C for 2 h. After wash with PBS, they were incubated with 1% osmium tetroxide at room temperature for 1 h, followed by dehydration with 30%–100% ethanol gradient. Next, the samples were infiltrated in 1:1 mixture of acetone and Epon 812 resin (SPI Supplies, West Chester, USA) overnight. Tissues were then embedded in araldite, sectioned with a diamond knife, stained with 1% uranyl acetate and 1% lead citrate, and examined with a transmission electron microscope (JME-1220; JEOL, Tokyo, Japan) at an acceleration voltage of 80 kV.

Periodic acid schiff (PAS) staining

Kidney tissues were fixed in 10% buffered formalin and embedded in paraffin. Paraffin-embedded histological sections were then cut into 5-μm sections, stained with PAS kit (Solarbio, Beijing, China) at room temperature for 2 h. After being washed with 1% ethanol hydrochloride, the slides were stained with eosin solution for 5 min and dehydrated with an alcohol gradient. Images were evaluated using light microscopy to determine the microscopic alterations of pathological significance.

Cell viability and actin cytoskeleton

Total cell number, as well as the number of viable and dead cells, is determined in parallel. The total cell number was determined by staining with Nuclei Dye, which stained the nuclei of live and dead cells. The percentage of dead cells is detected based on membrane permeability using the Dead Dye. Furthermore, viable cells are also stained with the Viable Dye. F-actin was stained using Phalloidin-iFluor™ 594 Conjugate (AAT Bioquest®, San Diego, USA), and podocytes were permeabilized for 5 min with PBS containing 0.1% Triton X-100 and then counterstained with 5 μg/mL of 4′,6-diami-

dino-2-phenylindole (DAPI). The images were acquired under a light microscope and fluorescence microscope (Olympus, Tokyo, Japan), respectively.

Flow cytometric analysis

After treatment, cell apoptosis was determined by using a commercial PE Annexin V Apoptosis Detection kit (BD Pharmingen, Franklin Lakes, USA). Briefly, cells were washed twice with cold PBS and then suspended at a concentration of 1×10^6 cells/mL. Then, 100 μL of the cell suspension (1×10^5 cells) was transferred to a 5-mL culture tube, and 5 μL of PE Annexin V and 5 μL 7-AAD were added into the cell suspension, followed by incubation at 25°C for 15 min in the dark. The percentages of PE Annexin V and/or 7-amino-actinomycin D (7-AAD)-positive cells were determined by flow cytometry.

Western blot analysis

Total protein was extracted from the kidney tissues or podocytes using lysis buffer (KeyGene, Nanjing, China). Western blot analysis was performed as previously described [25]. The antibodies used were as follows: Bax (21 kDa; 1:1000; Abcam, Cambridge, USA), Bcl-2 (26 kDa; 1:1000; Abcam), cleaved caspase 3 (17 kDa; 1:1000; Abcam), FOXA1 (51 kDa; 1:1000; Abcam), DNMT1 (183 kDa; 1:1000; Abcam), DNMT3a (108 kDa; 1:2000; Abcam), DNMT3b (96 kDa; 1:1000; Abcam) and β-actin (43 kDa; 1:1000; Zhongshan Biotech, Guangzhou, China). Image Lab software was used to analyze the signals. The relative protein expression was normalized by β-actin expression.

Quantitative real-time polymerase chain reaction (qRT-PCR)

Total RNA, including miRNA, was isolated using Trizol reagent (Invitrogen, Carlsbad, USA) according to the manufacturer's instructions. cDNA was synthesized with the First-Strand cDNA Synthesis kit (Thermo Scientific, Waltham, USA). qRT-PCR was performed as previously described [26]. The primers for *FOXA1* were synthesized by Sangon Biotech (Shanghai, China) and the sequences are as follows: *FOXA1* forward 5′-TACTCCTACATCTCGCTCATCA-3′ and reverse 5′-CCATGATCCACTGGTAGATCTC-3′; and *β-actin* forward 5′-AACAGTCCGCCTAGAAGCAC-3′, reverse 5′-CGTTGACATCCGTAAAGACC-3′. The primers for *miR-30a-5p* and *U6* were designed and synthesized by RiboBio (Guangzhou, China). All the experiments were performed in triplicates, and the data were normalized using *β-actin* or *U6* (for miRNA detection) as the house-keeping gene.

Nested methylation-specific-polymerase chain reaction (nMS-PCR)

Genomic DNA isolation and nMS-PCR were performed as previously described [26]. In briefly, genomic DNA was isolated from the kidney tissues using EZ DNA Methylation-Gold™ kit (Zymo Research, Irvine, USA). nMS-PCR consists of two-step PCR amplifications that are used for the detection methylation levels. The first step of nMS-PCR uses an outer primer pair set that does not contain any CpGs. The second step of PCR was carried out with a methylation primer and an unmethylated primer. The primers used for the nMS-PCR assays are listed in **Table 1**. The PCR products were separated by 2% agarose gel containing ethidium bromide and visualized with ultraviolet light.

TdT-mediated DUTP nick end labeling (TUNEL)

The apoptosis of podocytes was detected by using TUNEL apoptosis detection kit (Vazyme, Nanjing, China) according to the manufacturer's instructions. Cells were incubated with TUNEL reaction mixture at 37°C for 1 h. The number of TUNEL-positive nuclei (green) and the total number of nuclei (blue) in each field were scored, and apoptosis of podocytes were detected under the fluorescent microscope.

Luciferase reporter assay

The 2071 bp promoter region of miR-30a-5p was amplified by PCR and cloned into pGL3-basic vector (Yingbio Technology, Shanghai, China). The wild-type (WT) and corresponding mutated (Mut) versions of FOXA1 3′-UTR were cloned into pcDNA3.1 vector to get pcDNA-FOXA1-WT and pcDNA-FOXA1-Mut. HEK293T cells were seeded in 24-well plates, then the miR-30a-5p promoter reporter plasmids, pcDNA-FOXA1-WT and pcDNA-FOXA1-Mut, respectively were co-transfected with miR-30a-5p mimic into the cells using lipofectamine 2000 (Invitrogen). Forty-eight hour after transfection, luciferase activities were measured using the dual-luciferase reporter assay system (Promega, Madison, USA) according to the manufacturer's instructions, and normalized with *Renilla* luciferase activity.

Chromatin immunoprecipitation (ChIP)

ChIP assays were performed using the assay kit (Millipore, Billerica, USA) according to the manufacturer's instructions. Anti-DNMT1 antibody was used for chromatin immunoprecipitation. Primers were designed to detect the proximal promoter region of miR-30a-5p by qPCR as described previously [25]. The forward primer was 5′-AACGTTGACAGTGAGCGACT-3′ and the reverse primer was 5′-AGCTGCAAACATCCGACTGA-3′. IgG was used as a negative control to measure nonspecific background in immunoprecipitation.

MassARRAY quantitative methylation analysis

For every cleaved CpG site, the intensity of a pair of mass signals, one representing methylated and/or the other one representing unmethylated DNA, was recorded and analyzed using the Mass ARRAY EpiTYPER software. The relative methylation status was estimated by dividing the peak intensity, or area of the methylated

Table 1. Sequences of miR-30a-5 primers for nMS-PCR

Gene	Species	Primer sequence (5′→3′)
Outer primer	Mouse	Forward: GTTTATAGAATGTTGTTTGTATATTTTAGA Reverse: ATTTATAACTTCACAACTTCCAATC
Methylation primer	Mouse	Forward: TGTTTGTATATTTTAGAAATTTTCGT Reverse: TTTATAACTTCACAACTTCCAATCG
Unmethylation primer	Mouse	Forward: TGTTTGTATATTTTAGAAATTTTTGT Reverse: TATAACTTCACAACTTCCAATCAAA

DNA, by the sum of the intensities or areas of the methylated and unmethylated components. The ratios between methylated and unmethylated DNA were obtained as the quantity of methylation for further analysis.

Statistical analysis

All quantitative data were obtained from three independent experiments and presented as the mean ± SD. The results were analyzed using Graph Pad Prism 6.0 software. One-way ANOVA, Student-Newman-Keul's test (comparisons between multiple groups), or unpaired Student's *t*-test (between two groups) was used as appropriate. *P* values less than 0.05 were considered as statistically significant.

Results

HHcy induces glomerular damage and glomerular podocyte apoptosis *in vivo*

To examine the impact of HHcy on glomerular damage, we established HHcy mice by feeding *Cbs* mice with high-methionine diet for 8 weeks. As shown in Figure 1A, a high-methionine diet caused higher Hcy level in the serum of $Cbs^{+/-}$ mice compared with that in $Cbs^{+/+}$ mice, suggesting that HHcy model is successfully established. Meanwhile, the serum levels of blood urea nitrogen (BUN), creatinine (Cr) and cytochrome-C (Cyt C) were significantly increased in $Cbs^{+/-}$ mice (Figure 1B). Moreover, TEM images showed that glomerular podocytes in $Cbs^{+/-}$ mice have typical ultrastructural change, such as thickened ultrastructure of the glomerular basement membrane (red arrow), effacement and focal fusion of the podocyte foot process (blue arrow) (Figure 1C). PAS staining revealed HHcy-induced glomerular capillary collapse and mesangial expansion in $Cbs^{+/-}$ mice compared with those in $Cbs^{+/+}$ mice (Figure 1D). It has been reported that podocyte apoptosis is key to glomerular injury. By TUNEL staining, we showed that podocyte apoptosis in $Cbs^{+/-}$ mice was markedly increased compared with that in $Cbs^{+/+}$ mice (Figure 1E). Moreover, the ratio of Bax/Bcl-2 and expression of cleaved caspase-3 (c-caspase-3) were significantly increased in $Cbs^{+/-}$ mice (Figure 1F). These results indicated that HHcy induces glomerular damage and glomerular podocyte apoptosis *in vivo*.

Hcy induces glomerular damage and glomerular podocyte apoptosis *in vitro*

To further confirm the above results *in vitro*, actin filaments were labeled by phalloidin staining in podocytes treated with Hcy. The results showed a marked disruption of filamentous actin structure in the Hcy group compared with that in the control group (Figure

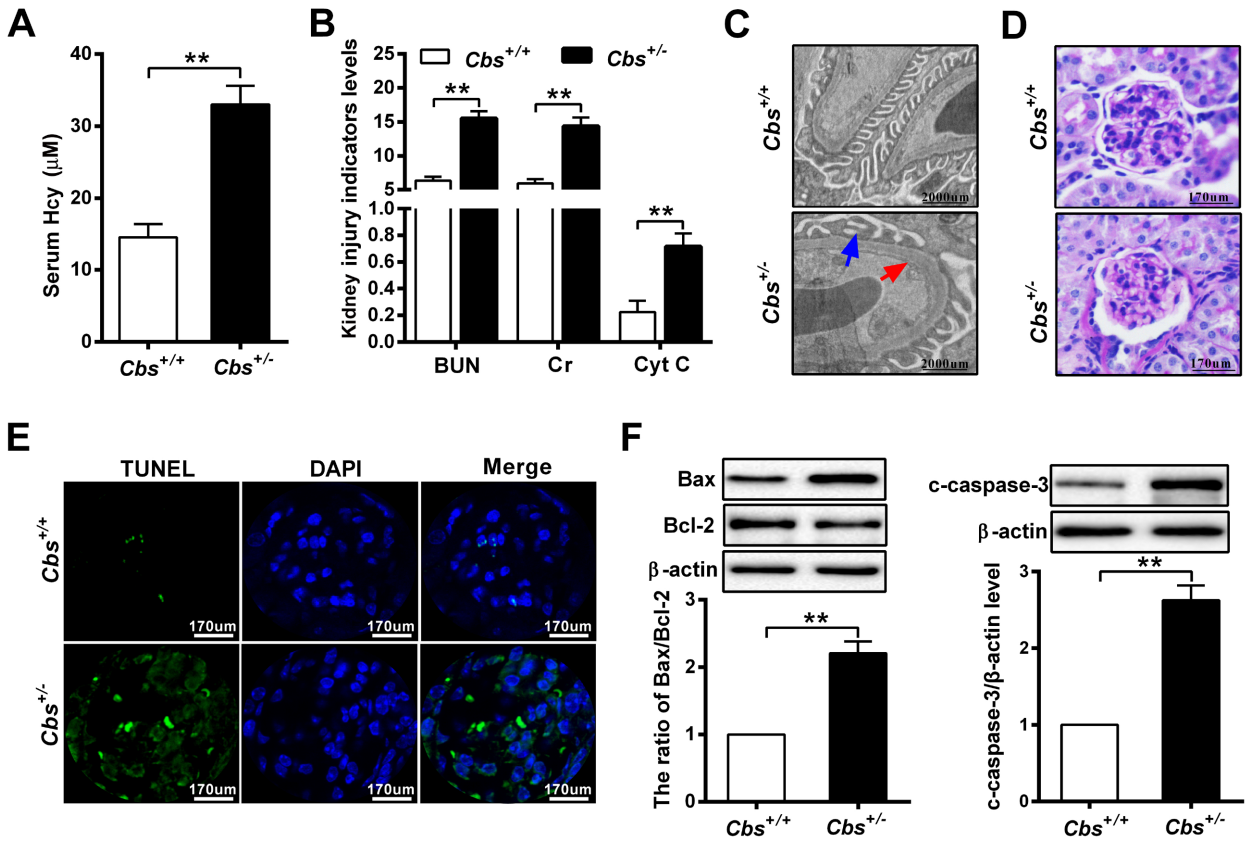

Figure 1. HHcy induces glomerular damage and glomerular podocyte apoptosis *in vivo* (A,B) The serum levels of Hcy, blood urea nitrogen (BUN), creatinine (Cr) and cytochrome-C (Cyt C) in $Cbs^{+/+}$ and $Cbs^{+/-}$ mice fed with high methionine diet were measured with an automatic biochemistry analyzer. *n*=6. (C) Transmission electron microscopy (TEM) was used to examine podocyte foot process changes in $Cbs^{+/-}$ mice (scale bar =2000 μm). Red arrow: thickened ultrastructure of the glomerular basement membrane; Blue arrow: effacement and focal fusion of the podocyte foot process. *n*=6. (D) Representative periodic acid schiff (PAS) staining images of glomerular structure change in $Cbs^{+/-}$ mice (scale bar=170 μm). *n*=6. (E) TUNEL staining assay showing podocyte apoptosis in $Cbs^{+/-}$ mice. Green fluorescence indicates TUNEL-positive cells and the nuclei were stained with DAPI (blue) (scale bar=170 μm). *n*=6. (F) The expressions of apoptosis-associated proteins Bax, Bcl-2 and cleaved caspase-3 (c-caspase-3) in $Cbs^{+/-}$ mice were detected by western blot analysis. *n*=6. Data are expressed as the mean ± SD. ***P*<0.01.

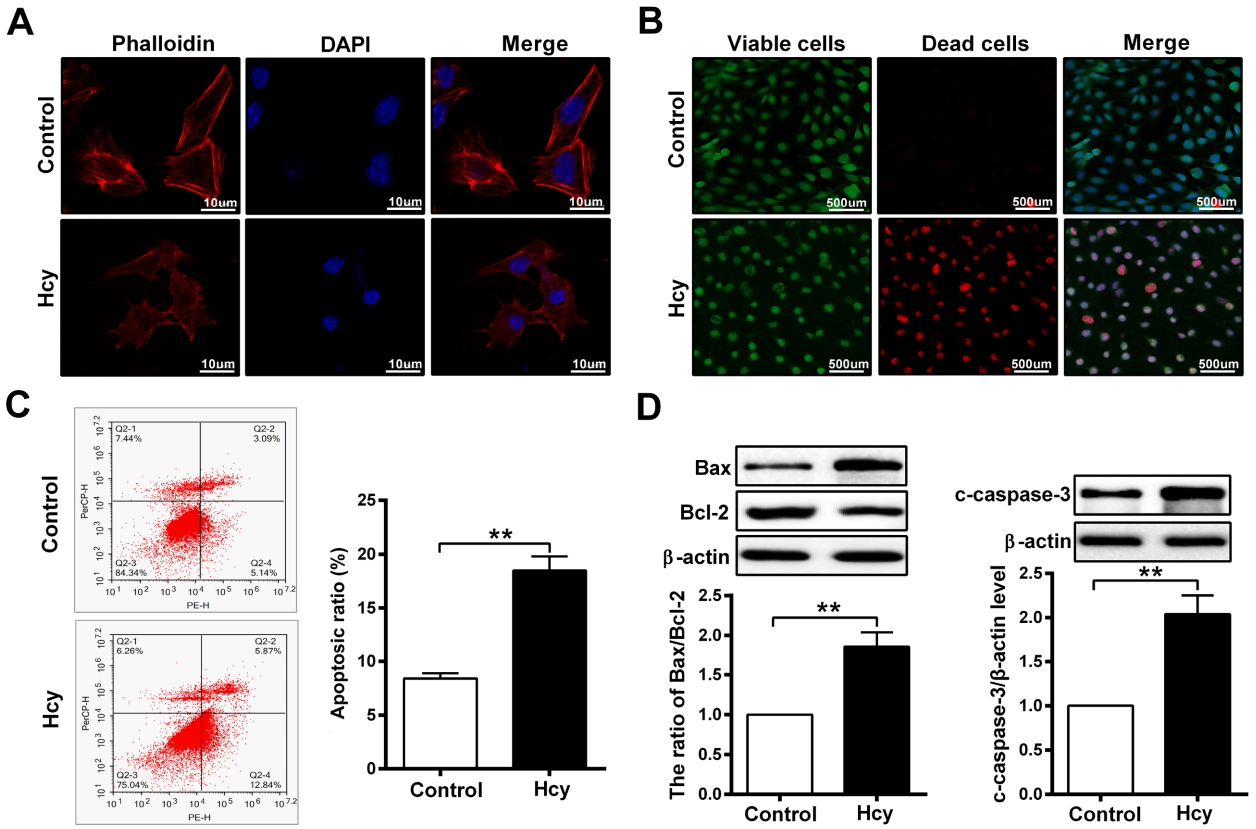

Figure 2. Hcy induces glomerular damage and glomerular podocyte apoptosis *in vitro* (A) Representative immunofluorescence images of podocytes stained with phalloidin (F-actin, red) and DAPI (nuclei staining, blue). Scale bar=10 μm. *n*=3. (B) Cell viability was determined after podocytes were treated with Hcy. Nuclei were stained with DAPI (blue), dead cells emitted red fluorescence and viable cells emitted green fluorescence. Scale bar=500 μm. *n*=3. (C) Flow cytometry analysis was used to evaluate and quantify podocyte apoptotic rate. *n*=3. (D) The protein expressions of Bax, Bcl-2 and c-caspase-3 in podocytes treated with Hcy were detected by western blot analysis. Data are expressed as the mean ± SD. *n*=3. ***P*<0.01.

2A). Meanwhile, the podocyte viability was decreased after Hcy treatment, showing obvious damage in podocytes induced by Hcy (Figure 2B). In addition, flow cytometric analysis showed that the apoptosis ratio of podocytes was significantly increased in the Hcy group (Figure 2C). Western blot analysis results further showed increased expressions of Bax and c-caspase-3 and decreased expression of Bcl-2 in podocytes treated with Hcy (Figure 2D). These results confirmed that Hcy induced apoptosis of podocytes *in vitro*, which was consistent with the *in vivo* results.

miR-30a-5p is downregulated during Hcy-induced podocyte apoptosis

In order to investigate whether miR-30a-5p is involved in Hcy-induced podocyte apoptosis, we detected the expression of miR-30a-5p in $Cbs^{+/-}$ mice fed with high-methionine diet and in podocytes treated with Hcy. The expression of miR-30a-5p was significantly reduced both in glomeruli of $Cbs^{+/-}$ mice and in podocytes treated with Hcy (Figure 3). These data suggested that Hcy downregulates miR-30a-5p expression both *in vivo* and *in vitro*.

miR-30a-5p inhibits Hcy-induced podocyte apoptosis both *in vitro* and *in vivo*

To explore the role of miR-30a-5p in Hcy-induced podocyte apoptosis, we transfected miRNA negative control (miR-neg), miR-30a-5p mimic or miR-30a-5p inhibitor into podocytes with high efficacy

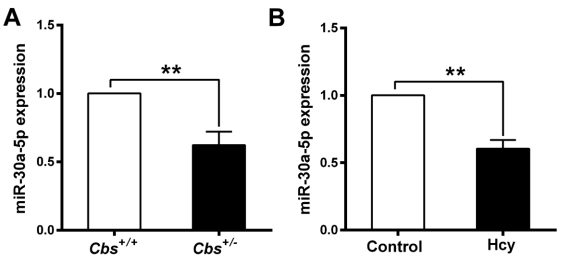

Figure 3. miR-30a-5p is downregulated during Hcy-induced podocyte apoptosis (A,B) The expression of miR-30a-5p was analyzed by qRT-PCR in $Cbs^{+/-}$ mice (*n*=6) and in podocytes treated with Hcy (*n*=3). Data are expressed as the mean ± SD. ***P*<0.01.

as confirmed by qRT-PCR (Supplementary Figure S1). Flow cytometric analysis showed that miR-30a-5p mimic inhibited the apoptosis of podocytes treated with Hcy, which could be reversed by miR-30a-5p inhibitor transfection (Figure 4A). Similarly, western blot analysis showed that both the ratio of Bax/Bcl-2 and c-caspase-3 protein expression were decreased after transfection with miR-30a-5p mimic in podocytes treated with Hcy. In contrast, miR-30a-5p inhibitor transfection increased the ratio of Bax/Bacl-2 and c-caspase-3 protein expression (Figure 4B). Furthermore, to examine whether miR-30a-5p regulates podocyte apoptosis *in vivo*, recombinant adeno-associated virus serotype 9 (AAV9) vectors har-

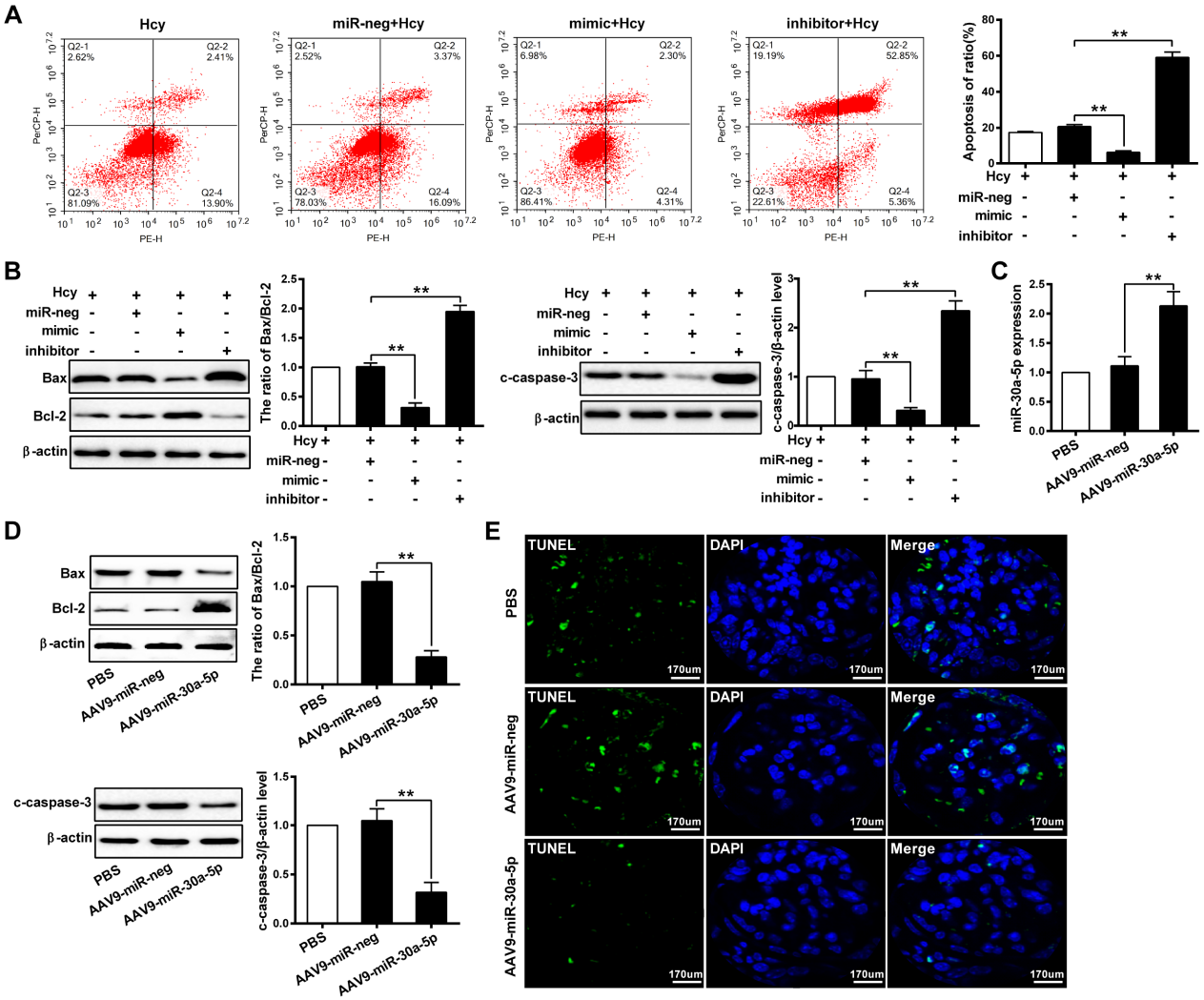

Figure 4. miR-30a-5p inhibits podocyte apoptosis during HHcy-induced glomerular injury (A) Flow cytometry analysis was used to detect apoptosis of podocytes after transfected with miR-neg, miR-30a-5p mimic or miR-30a-5p inhibitor in presence of Hcy, respectively. *n*=3. (B) The protein expressions of Bax, Bcl-2 and c-caspase-3 were detected by western blot analysis in podocytes transfected with miR-neg, miR-30a-5p mimic or miR-30a-5p inhibitor and treated with Hcy. *n*=3. (C) The expression of miR-30a-5p was analyzed by qRT-PCR after AAV9-miR-30a-5p was delivered into kidney of *Cbs*$^{+/-}$ mice by intraparenchymal injections. *n*=6. (D) Representative western blots and quantification results of Bax, Bcl-2 and c-caspase-3 in the glomerulus after AAV9-miR-30a-5p or AAV9-miR-neg was delivered into kidney of *Cbs*$^{+/-}$ mice. *n*=6. (E) The apoptotic podocytes in glomerulus were detected by TUNEL assay after AAV9-miR-30a-5p was delivered into kidney of *Cbs*$^{+/-}$ mice by intraparenchymal injections. Scale bar=170 μm. Data are expressed as the mean ± SD. *n*=6. ***P*<0.01.

boring miR-30a-5p (AAV9-miR-30a-5p) were delivered into the kidney of *Cbs*$^{+/-}$ mice by intraparenchymal injection (Figure 4C). Western blot and TUNEL analysis results showed that the apoptosis of podocytes was significantly decreased in AAV9-miR-30a-5p mice than that in AAV9-miR-neg mice (Figure 4D,E). These results indicated that overexpression of miR-30a-5p inhibits Hcy-induced podocyte apoptosis.

FOXA1 is a target gene of miR-30a-5p

To further explore the regulation mechanisms of miR-30a-5p in podocyte apoptosis induced by Hcy, we identified the potential targets of miR-30a-5p using Targetscan online software (http://www.targetscan.org/vert_72/). Interestingly, we found that miR-30a-5p has complementary binding sites to the 3′-UTR of FOXA1 (Figure 5A). To elucidate whether FOXA1 is a target of miR-30a-5p, we constructed wild-type (WT) and mutant (Mut) FOXA1 reporter plasmids. Co-expression of miR-30a-5p and WT reporter plasmids significantly reduced the luciferase activity, while co-expression of miR-30a-5p and mutated FOXA1 reporter did not change the luciferase activity (Figure 5B). These results indicated that miR-30a-5p directly targets FOXA1. In addition, the mRNA and protein expression of FOXA1 were increased both in glomeruli of *Cbs*$^{+/-}$ mice fed with high-methionine diet and in podocytes treated with Hcy (Figure 5C,D). Thereafter, the results of western blot analysis revealed that overexpression of miR-30a-5p suppressed the protein expression of FOXA1 in podocytes treated with Hcy, while silencing of miR-30a-5p promoted the protein expression of FOXA1 (Figure 5E). Similar results were also obtained in AAV9-miR-30a-5p mice (Figure 5F). These results indicated that miR-30a-5p directly binds to the FOXA1 3′-UTR to inhibit FOXA1 expression in Hcy-induced

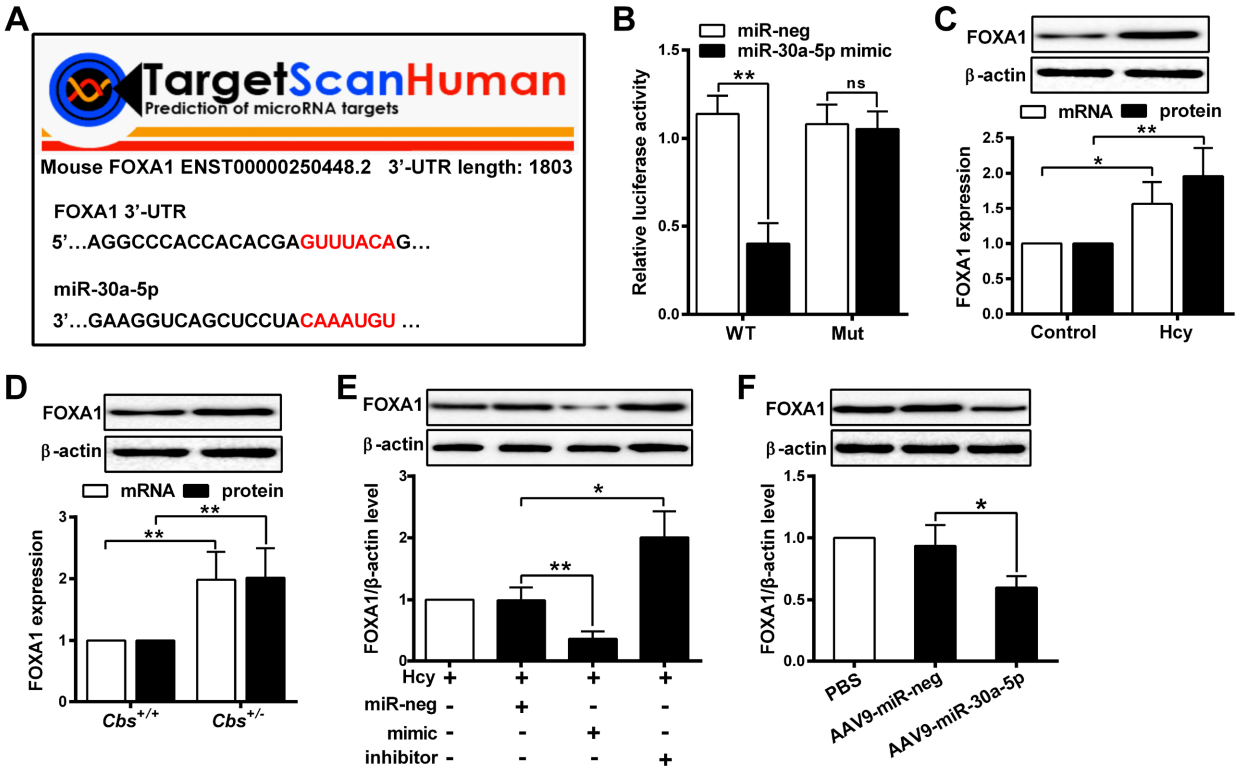

Figure 5. ***FOXA1* is a target gene of miR-30a-5p** (A) A schematic diagram showing the predicted miR-30a-5p binding sites in the 3′-UTR of *FOXA1*. (B) The reporter vectors containing wild-type (WT) 3′-UTR of FOXA1 or its mutant (Mut) were co-transfected with miR-neg or miR-30a-5p mimic. Relative luciferase activities were normalized by the ratio of firefly and Renilla luciferase activities. *n*=3. (C,D) The expression of FOXA1 was analyzed by qRT-PCR and western blot analysis in $Cbs^{+/-}$ mice or podocytes treated with Hcy. *n*=3. (E) Western blot analysis of FOXA1 protein expression after podocytes were transfected with miR-neg, miR-30a-5p mimic or miR-30a-5p inhibitor in presence of Hcy. *n*=3. (F) Representative western blots and quantification results of FOXA1 in the glomerulus after AAV9-miR-30a-5p was delivered into kidney of $Cbs^{+/-}$ mice. Data are expressed as the mean ± SD. *n*=6. **P*<0.05, ***P*<0.01.

podocyte apoptosis.

Hcy promotes DNA methylation of miR-30a-5p promoter in podocytes

A possible mechanism of miRNA transcription regulation is DNA methylation [27]. To further investigate whether downregulation of miR-30a-5p in Hcy-induced podocyte apoptosis is related to DNA methylation, several fragments of miR-30a-5p promoter region (−2000/+71, −1400/+71, −921/+71, and −600/+71) were inserted into the firefly luciferase vector pGL3. The dual-luciferase reporter assay showed that the region between −1400 and −921 of miR-30a-5p promoter region has the highest activity, indicating that the region between −1400 and −921 of miR-30a-5p promoter is critical for miR-30a-5p expression (Figure 6A). nMS-PCR results showed that the methylation level of the miR-30a-5p promoter in the glomeruli of $Cbs^{+/-}$ mice is higher than that of $Cbs^{+/+}$ mice (Figure 6B). In addition, MassARRAY quantitative methylation analysis showed that the methylation level of miR-30a-5p promoter was increased in podocytes treated with Hcy (Figure 6C). To further examine whether DNA methylation directly represses miR-30a-5p promoter activity, the cloned miR-30a-5p promoter fragments were methylated by SssI DNA methylase (SssI), and proper methylation sites of miR-30a-5p promoter were confirmed by digestion with methylation-specific restriction enzyme McrBC. The dual-luciferase reporter assay results showed that miR-30a-5p promoter activity was markedly blocked after treatment with M.SssI (Figure 6D). These results suggested that miR-30a-5p transcription level was modulated by DNA methylation in Hcy-induced podocyte apoptosis.

DNMT1 inhibits miR-30a-5p transcription activity in podocytes in a DNA methylation-dependent manner

DNA methylation is mediated by DNMT family members DNMT1, DNMT3a and DNMT3b [28]. To explore their roles in miR-30a-5p DNA methylation induced by Hcy, we examined the expressions of DNMT1, DNMT3a and DNMT3b both *in vivo* and *in vitro*. As shown in Figure 7A,B, the expressions of DNMT1, DNMT3a and DNMT3b were increased both in the glomeruli of $Cbs^{+/-}$ mice and in podocytes treated with Hcy. Moreover, only DC_05 (DNMT1 specific inhibitor) showed the strongest stimulatory effect on miR-30a-5p expression, while all investigated inhibitors, including 5-Azacytidine (AZC, DNMT inhibitor), theaflavin 3, −3′-digallate (TFD, DNMT3a specific inhibitor) and nanaomycin A (NA, DNMT3b specific inhibitor), did not change miR-30a-5p expression (Figure 7C). This result suggested that DNMT1 is the major regulator for miR-30a-5p methylation induced by Hcy. To further investigate the regulatory effect of DNMT1 on miR-30a-5p expression, we knocked down or overexpressed DNMT1 in podocytes by DNMT1 siRNA (si-DNMT1) or recombinant adenoviruses expressing DNMT1 (Ad-DNMT1) respectively (Supplementary Figure S2). As shown in Figure 7D, overexpression of DNMT1 significantly decreased the expression of miR-30a-5p in podocytes treated with Hcy. In contrast, knockdown of DNMT1 increased the expression of

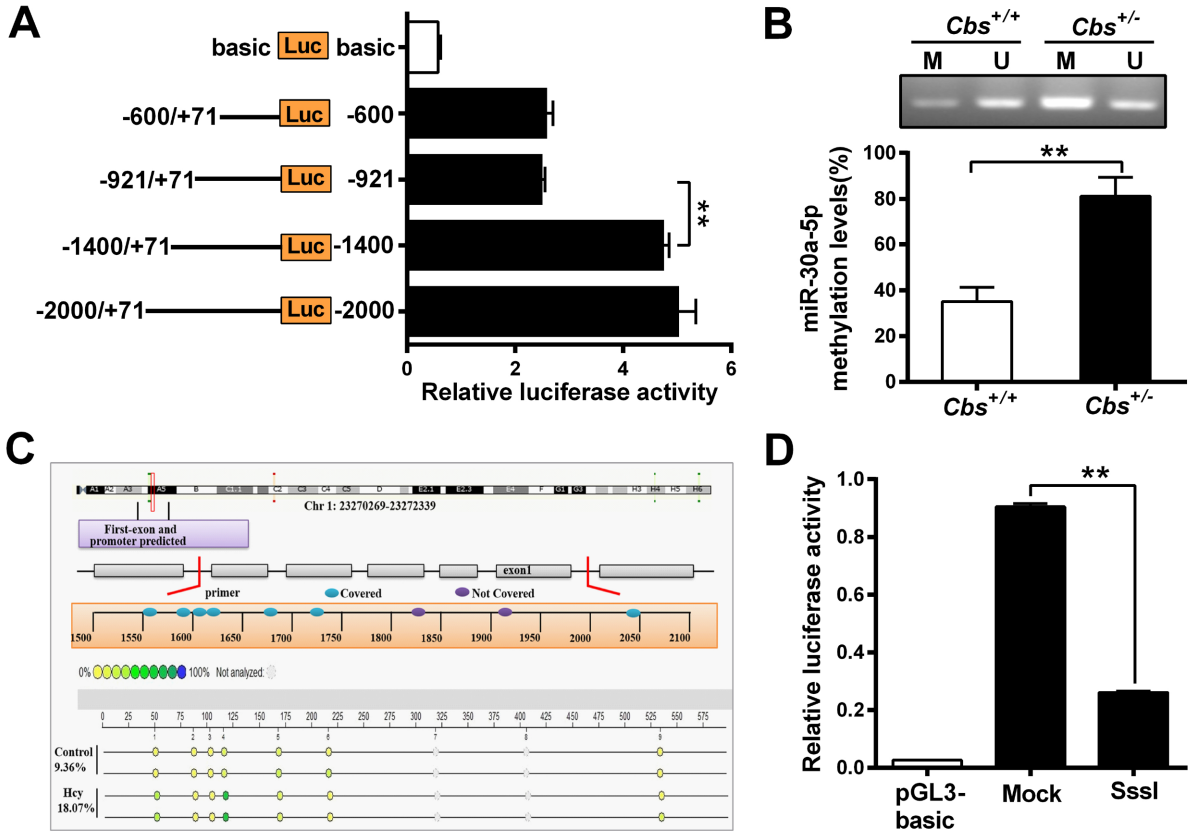

Figure 6. Hcy promotes DNA methylation of miR-30a-5p promoter in podocyte (A) The promoter activity of the miR-30a-5p was examined by dual-luciferase reporter assay. Fragments of the miR-30a-5p promoter (–2000/+71, –1400/+71, –921/+71, and –600/+71) were co-transfected into HEK293 cells with a *Renilla* luciferase vector. The results were presented as firefly luciferase activity normalized to Renilla luciferase activity 48 h after transfection. *n*=3. (B) Methylation level of the miR-30a-5p promoter region in *Cbs*$^{+/+}$ and *Cbs*$^{+/-}$ mice was analyzed by nMS-PCR. M: methylated status; U: unmethylated status. *n*=6. (C) MassARRAY quantitative methylation analysis of DNA methylation level of miR-30a-5p promoter region in podocytes treated with Hcy. *n*=3. (D) The proximal promoter region –2000/+71 of miR-30a-5p was methylated using methylase SssI *in vitro* and cloned into a luciferase reporter vector. The promoter activity of the methylated miR-30a-5p proximal promoter region was assessed by transfection of the luciferase reporter vectors into HEK293 cells. Data are expressed as the mean ± SD. *n*=3. ***P*<0.01.

miR-30a-5p. In addition, the methylation level of miR-30a-5p promoter in Hcy-treated podocytes was significantly decreased after DC_05 treatment or DNMT1 knockdown, while overexpression of DNMT1 enhanced the miR-30a-5p promoter methylation level (Figure 7E). These results revealed that DNMT1 can inversely regulate miR-30a-5p expression. Furthermore, we examined that whether DNMT1 binds to miR-30a-5p promoter directly *in vitro*. ChIP analysis showed that Hcy enhanced the binding of DNMT1 to the miR-30a-5p promoter (Figure 7F). We further found that overexpression of DNMT1 significantly promoted the enrichment of DNMT1 to miR-30a-5p promoter in podocytes treated with Hcy, whereas this phenomenon was decreased by DNMT1 knockdown (Figure 7G). Taken together, these results demonstrated that DNMT1 promotes miR-30a-5p methylation by direct binding to the miR-30a-5p promoter.

Discussion

In the present study, we established HHcy *Cbs*$^{+/-}$ mice model with a serum level of Hcy around 40 μM. The results showed that HHcy aggravates glomerular podocyte injury and apoptosis in *Cbs*$^{+/-}$ mice, and similar results were obtained in podocytes treated with Hcy *in vitro*, suggesting that elevated Hcy level is associated with glomerular podocyte injury.

To explore the mechanism of HHcy-induced glomerular podocyte injury, we focused on miRNAs due to their regulating function in most biological processes of cells, including cell proliferation, differentiation, senescence and apoptosis [29]. miRNAs are a class of non-coding small RNA molecules, which regulate gene expression by completely or partially binding to the 3′-UTR of the target mRNAs. However, the mechanism responsible for miRNA regulation and the contributions of Hcy-regulated miRNAs towards HHcy-induced glomerular injury has not been well explored. Previous studies showed that miRNAs plays an important role in the occurrence and development of various kidney diseases, especially in the maintenance of glomerular function. miR-770-5p is involved in the development of diabetic nephropathy through regulating podocyte apoptosis [30,31]. In addition, miR-382 was found to inhibit glomerular mesangial cell proliferation and extracellular matrix accumulation in diabetic nephropathy by targeting *FOXO1* [32]. In this study, we showed that Hcy inhibits miR-30a-5p expression both *in vitro* and *in vivo*. Furthermore, we found that FOXA1 is a direct target of miR-30a-5p by using miRNA target gene prediction tools and bioinformatics-based analyses. In addition, our study highlighted the functional role of miR-30a-5p in HHcy-induced glomerular injury. We found that podocyte apoptosis caused by Hcy were alleviated by overexpression of miR-30a-5p, and recombinant

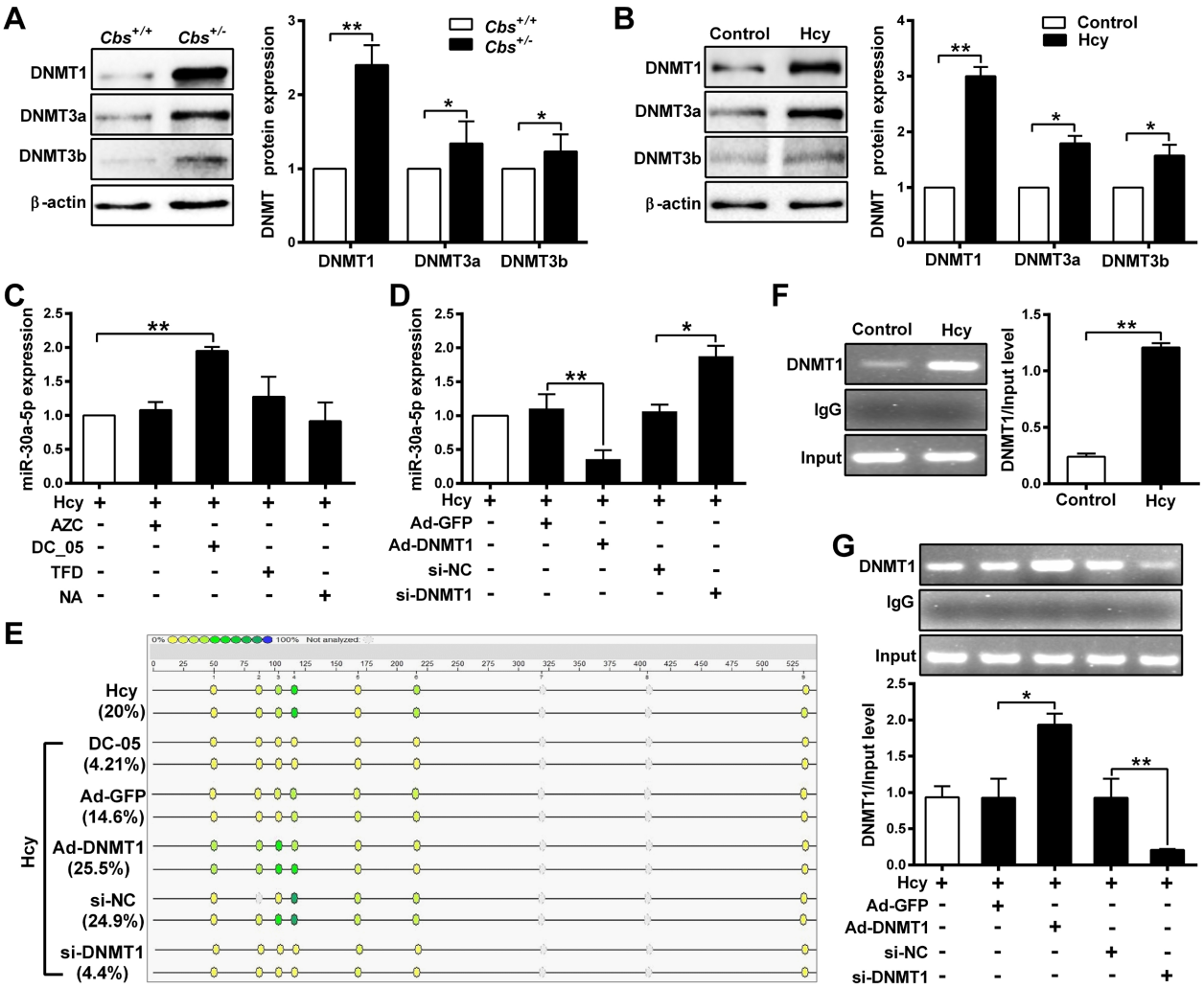

Figure 7. DNMT1 inhibits miR-30a-5p transcriptional activities in podocytes in a DNA methylation-dependent manner (A,B) Western blot analysis of DNMT1, DNMT3a and DNMT3b protein expressions in *Cbs*$^{+/-}$ mice (n=6) and Hcy-treated podocytes (n=3). (C) The expression of miR-30a-5p was detected in podocytes after treatment with AZC, DC_05, theaflavin 3,3′-digallate (TFD) or NanaomycinA (NA) (DNMTs, DNMT1, DNMT3a and DNMT3b specific inhibitors, respectively) for 48 h. n=3. (D) The relative expression of miR-30a-5p in Hcy-treated podocytes with overexpression or knockdown of DNMT1. n=3. (E) MassARRAY quantitative methylation analysis of DNA methylation level of miR-30a-5p promoter region after overexpression or knockdown DNMT1 in Hcy-treated podocytes. n=3. (F,G) ChIP assay revealed the fold enrichment of DNMT1 on miR-30a-5p promoter. The normal mouse IgG was used as a negative control. Data are expressed as the mean ± SD. n=3. *P<0.05, **P<0.01.

adeno-associated viral vectors AAV9 harboring miR-30-5p protected podocyte apoptosis *in vivo*. These data provided a novel mechanism responsible for HHcy-induced glomerular podocyte injury by regulating miR-30a-5p expression.

DNA methylation is often regulated by the activities of key enzymes and intermediate metabolites including Hcy which is an amino acid produced in the metabolism of methionine [20,33]. Our previous study showed that abnormal DNA methylation is closely associated with the pathogenesis of liver diseases and atherosclerosis [21,25]. Meanwhile, the strong evidence that Hcy can increase DNA methylation prompted us to evaluate the relationship between DNA methylation, Hcy, and miR-30a-5p. As expected, DNA methylation of the miR-30a-5p promoter was significantly increased in *Cbs*$^{+/-}$ mice and in glomerular podocytes induced by Hcy, and the region between −1400 and −921 of miR-30a-5p promoter played a key role for its transcription regulation, suggesting that downregulation of miR-30a-5p is mediated in a DNA methylation-dependent manner.

DNMTs are responsible for establishing and maintaining DNA methylation in mammalian cells and increased DNMT activity leads to the hypermethylation of cellular genes and miRNAs, which are generally associated with transcriptional repression and thereby contribute to gene regulation [34]. In this study, we observed that the protein levels of DNMT1, DNMT3a and DNMT3b were increased both *in vivo* and *in vitro*. Subsequent experiments further suggested that DNMT1 is the major regulator for DNA methylation of miR-30a-5p promoter. The present study further uncovered that overexpression of DNMT1 significantly decreases miR-30a-5p expression by increasing its methylation. More importantly, ChIP analysis indicated that Hcy enhances the binding of DNMT1 with the miR-30a-5p promoter, and the binding is more obvious when DNMT1 is overexpressed in podocytes treated with Hcy.

In conclusion, the present study demonstrates that overexpression of miR-30a-5p hampers the development and progres-

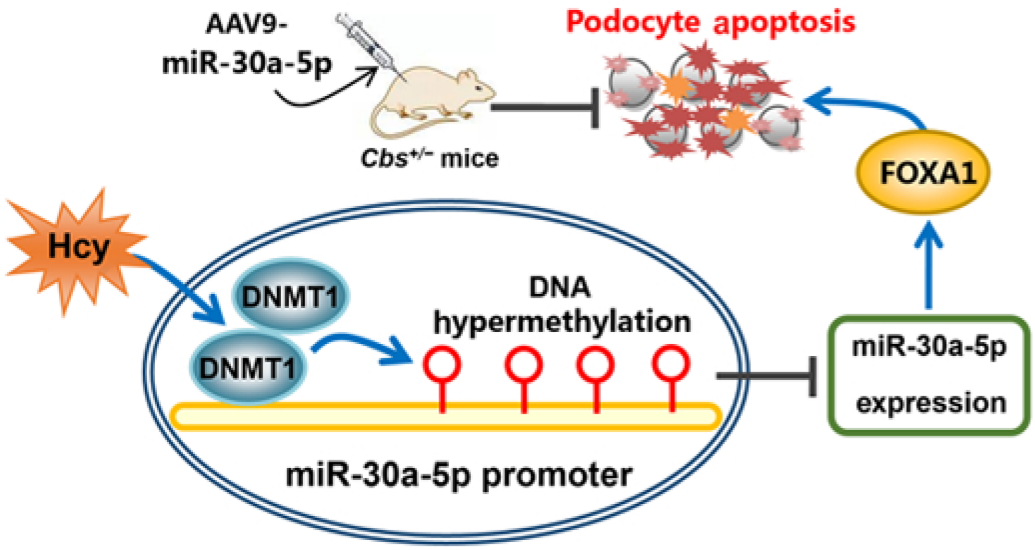

Figure 8. Downregulation of miR-30a-5p promotes glomerular podocyte apoptosis via DNMT1 mediates hypermethylation under hyperhomocysteinemia Overexpression of miR-30a-5p inhibits Hcy induced-podocyte apoptosis both *in vivo* and *in vitro*. Mechanistically, DNMT1 mediates miR-30a-5p promoter hypermethylation to inhibits miR-30a-5p transcription, and thereby regulates *FOXA1* expression.

sion of Hcy-induced glomerular podocyte injury by targeting FOXA1. Mechanistically, DNMT1-mediated DNA hypermethylation promotes Hcy-induced podocyte injury by downregulation of miR-30a-5p expression, suggesting a new pathogenic pathway in HHcy-associated CKD (Figure 8).

Supplementary Data

Supplementary data is available at *Acta Biochimica et Biophysica Sinica* online.

Funding

This work was supported by the grants from the National Natural Science Foundation of China (Nos. 81960094, 81900273, 81760139, and 82060139), the Key Research and Development Projects in Ningxia (Nos. 2018BEG02004 and 2019BFG02004), the Natural Science Foundation of Ningxia (Nos. 2020AAC02021 and 2020AAC02038).

Conflict of Interest

The authors declare that they have no conflict of interest.

References

1. Jakubowski H. Homocysteine modification in protein structure/function and human disease. *Physiol Rev* 2019, 99: 555-604
2. Ostrakhovitch EA, Tabibzadeh S. Homocysteine in chronic kidney disease. *Adv Clin Chem* 2015, 72: 77-106
3. Conley SM, Abais-Battad JM, Yuan X, Zhang Q, Boini KM, Li PL. Contribution of guanine nucleotide exchange factor Vav2 to NLRP3 inflammasome activation in mouse podocytes during hyperhomocysteinemia. *Free Radical Biol Med* 2017, 106: 236–244
4. Zhang Q, Conley SM, Li G, Yuan X, Li PL. Rac1 GTPase inhibition blocked podocyte injury and glomerular sclerosis during hyperhomocysteinemia via suppression of nucleotide-binding oligomerization domain-like receptor containing pyrin domain 3 inflammasome activation. *Kidney Blood Press Res* 2019, 44: 513–532
5. Liu XD, Zhang LY, Zhu TC, Zhang RF, Wang SL, Bao Y. Overexpression of miR-34c inhibits high glucose-induced apoptosis in podocytes by targeting Notch signaling pathways. *Int J Clin Exp Pathol* 2015, 8: 4525-4534
6. Assady S, Benzing T, Kretzler M, Skorecki KL. Glomerular podocytes in kidney health and disease. *Lancet* 2019, 393: 856–858
7. Carney EF. Podocyte biology: dynamic control of actin remodelling. *Nat Rev Nephrol* 2016, 12: 650
8. Sun Z, Shi K, Yang S, Liu J, Zhou Q, Wang G, Song J, *et al.* Effect of exosomal miRNA on cancer biology and clinical applications. *Mol Cancer* 2018, 17: 147
9. Gebeshuber CA, Kornauth C, Dong L, Sierig R, Seibler J, Reiss M, Tauber S, *et al.* Focal segmental glomerulosclerosis is induced by microRNA-193a and its downregulation of WT1. *Nat Med* 2013, 19: 481–487
10. Zhang X, Song S, Luo H. Regulation of podocyte lesions in diabetic nephropathy via miR-34a in the Notch signaling pathway. *Medicine* 2016, 95: e5050
11. Chen YQ, Wang XX, Yao XM, Zhang DL, Yang XF, Tian SF, Wang NS. MicroRNA-195 promotes apoptosis in mouse podocytes via enhanced caspase activity driven by BCL2 insufficiency. *Am J Nephrol* 2011, 34: 549–559
12. Fan WX, Wen XL, Xiao H, Yang QP, Liang Z. MicroRNA-29a enhances autophagy in podocytes as a protective mechanism against high glucose-induced apoptosis by targeting heme oxygenase-1. *Eur Rev Med Pharmacol Sci* 2018, 22: 8909-8917
13. Jin LW, Pan M, Ye HY, Zheng Y, Chen Y, Huang WW, Xu XY, *et al.* Downregulation of the long non-coding RNA XIST ameliorates podocyte apoptosis in membranous nephropathy via the miR-217-TLR4 pathway. *Exp Physiol* 2019, 104: 220-230
14. Ma J, Li YT, Zhang SX, Fu SZ, Ye XZ. MiR-590-3p attenuates acute kidney injury by inhibiting tumor necrosis factor receptor-associated factor 6 in septic mice. *Inflammation* 2019, 42: 637–649
15. Mao L, Liu S, Hu L, Jia L, Wang H, Guo M, Chen C, *et al.* miR-30 family: a promising regulator in development and disease. *Biomed Res Int* 2018, 2018: 9623412
16. Wu J, Zheng C, Fan Y, Zeng C, Chen Z, Qin W, Zhang C, *et al.* Downregulation of microRNA-30 facilitates podocyte injury and is prevented by glucocorticoids. *J Am Soc Nephrol* 2014, 25: 92–104
17. Yang R, Hong H, Wang M, Ma Z. Correlation between single-nucleotide polymorphisms within miR-30a and related target genes and risk or

prognosis of nephrotic syndrome. *DNA Cell Biol* 2018, 37: 233–243
18. Field AE, Robertson NA, Wang T, Havas A, Ideker T, Adams PD. DNA methylation clocks in aging: categories, causes, and consequences. *Mol Cell* 2018, 71: 882–895
19. Greenberg MVC, Bourc'his D. The diverse roles of DNA methylation in mammalian development and disease. *Nat Rev Mol Cell Biol* 2019, 20: 590–607
20. Li JG, Barrero C, Gupta S, Kruger WD, Merali S, Praticò D. Homocysteine modulates 5-lipoxygenase expression level via DNA methylation. *Aging Cell* 2017, 16: 273–280
21. Yang A, Jiao Y, Yang S, Deng M, Yang X, Mao C, Sun Y, ***et al.*** Homocysteine activates autophagy by inhibition of CFTR expression via interaction between DNA methylation and H3K27me3 in mouse liver. *Cell Death Dis* 2018, 9: 169
22. Yang A, Sun Y, Gao Y, Yang S, Mao C, Ding N, Deng M, ***et al.*** Reciprocal regulation between miR-148a/152 and DNA methyltransferase 1 is associated with hyperhomocysteinemia-accelerated atherosclerosis. *DNA Cell Biol* 2017, 36: 462–474
23. Torres-Ferreira J, Ramalho-Carvalho J, Gomez A, Menezes FD, Freitas R, Oliveira J, Antunes L, ***et al.*** MiR-193b promoter methylation accurately detects prostate cancer in urine sediments and miR-34b/c or miR-129-2 promoter methylation define subsets of clinically aggressive tumors. *Mol Cancer* 2017, 16: 26
24. Li T, Li Y, Gan Y, Tian R, Wu Q, Shu G, Yin G. Methylation-mediated repression of MiR-424/503 cluster promotes proliferation and migration of ovarian cancer cells through targeting the hub gene KIF23. *Cell* 2019, 18: 1601-1618
25. Xu L, Hao H, Hao Y, Wei G, Li G, Ma P, Xu L, ***et al.*** Aberrant MFN2 transcription facilitates homocysteine-induced VSMCs proliferation via the increased binding of c-Myc to DNMT1 in atherosclerosis. *J Cell Mol Med* 2019, 23: 4611–4626
26. Zhang HP, Wang YH, Ma SC, Zhang H, Yang AN, Yang XL, Zhang MH, ***et al.*** Homocysteine inhibits endothelial progenitor cells proliferation via DNMT1-mediated hypomethylation of Cyclin A. *Exp Cell Res* 2018, 362: 217–226
27. Cao CJ, Zhang HP, Zhao L, Zhou L, Zhang M, Xu H, Han X, ***et al.*** miR-125b targets DNMT3b and mediates p53 DNA methylation involving in the vascular smooth muscle cells proliferation induced by homocysteine. *Exp Cell Res* 2016, 347: 95–104
28. Lyko F. The DNA methyltransferase family: a versatile toolkit for epigenetic regulation. *Nat Rev Genet* 2018, 19: 81-92
29. Piscopo P, Lacorte E, Feligioni M, Mayer F, Crestini A, Piccolo L, Bacigalupo I, ***et al.*** MicroRNAs and mild cognitive impairment: A systematic review. *Ageing Res Rev* 2019, 50: 131–141
30. Kabekkodu SP, Shukla V, Varghese VK, D′ Souza J, Chakrabarty S, Satyamoorthy K. Clustered miRNAs and their role in biological functions and diseases. *Biol Rev* 2018, 93: 1955–1986
31. Zhang SZ, Qiu XJ, Dong SS, Zhou LN, Zhu Y, Wang MD, Jin LW. MicroRNA-770-5p is involved in the development of diabetic nephropathy through regulating podocyte apoptosis by targeting TP53 regulated inhibitor of apoptosis 1. *Eur Rev Med Pharmacol Sci* 2019, 23: 1248-1256
32. Wang S, Wen X, Han XR, Wang YJ, Shen M, Fan SH, Zhuang J, ***et al.*** Repression of microRNA-382 inhibits glomerular mesangial cell proliferation and extracellular matrix accumulation via FoxO1 in mice with diabetic nephropathy. *Cell Prolif* 2018, 51: e12462
33. Harris CJ, Scheibe M, Wongpalee SP, Liu W, Cornett EM, Vaughan RM, Li X, ***et al.*** A DNA methylation reader complex that enhances gene transcription. *Science* 2018, 362: 1182–1186
34. Schmitz RJ, Lewis ZA, Goll MG. DNA methylation: shared and divergent features across eukaryotes. *Trends Genet* 2019, 35: 818–827